Enhancing Figure of Merit of $Bi_{0.5}Sb_{1.5}Te_3$ Through Nano-composite Approach

HUNG CHANG HSU, JING-YI HUANG and TSAI-KUN HUANG

New Materials Research & Development Department
China Steel Corporation

$Bi_{0.5}Sb_{1.5}Te_3$ nano-composites were fabricated through a hot pressing process, where powder was prepared by mixing various ratios (0, 20, 40 and 100 wt%) of micro-grain and nano-grain $Bi_{0.5}Sb_{1.5}Te_3$ powder. The micro-grain powder was obtained by grinding a zone-melting $Bi_{0.5}Sb_{1.5}Te_3$ ingot. The nano-grain powder was obtained by grinding a melt-spun $Bi_{0.5}Sb_{1.5}Te_3$ ribbon. The melt spun ribbons are composed of 5-10 nm nano-grains. The microstructure of the $Bi_{0.5}Sb_{1.5}Te_3$ nano-composite shows that the micro-grain powder is surrounded by the melt spun powder. The grain size of the melt spun powder remained the same after hot pressing. The highest figure of merit, ZT_{max}~1.2@400K, was obtained for $Bi_{0.5}Sb_{1.5}Te_3$ nano-composite with mixing 40 wt% of melt-spun powder. After further annealing at 300℃, ZT was enhanced to 1.42. A SEM image shows there are aggregated Te-rich precipitations in the annealed sample. The aggregated Te-rich precipitations could result in a carrier energy filtering effect leading to the increase of the Seebeck coefficient, from 188 to 236 V/K at room temperature.

Keywords*: Bi_2Te_3, Nano-composite, Nano-precipatation*

1. INTRODUCTION

Thermoelectric (TE) materials directly convert heat to electricity. Near room temperature, Bi_2Te_3 is the most suitable thermoelectric material[1]. The thermoelectric efficiency is associated with the thermoelectric figure of merit (ZT), which is defined as $ZT = S^2\sigma T / \kappa$, where S, σ, κ and T are the Seebeck coefficient, electrical conductivity, thermal conductivity and absolute temperature, respectively. The larger the ZT value, the higher the energy conversion efficiency of a TE material. For the purpose of enhancing ZT, Researchers have tried to increase S and σ or decrease κ.

Many groups have tried to manipulate the carrier concentration[2-4] and change the annealing condition[5-9] for the purpose of electrical conductivity enhancement. But κ was increased at the same time. Because κ is composed of electron (κ_e) and phonon (κ_{ph}) contributions. Although σ is enhanced, κ_e is also increased. Consequently, the enhancement of ZT is limited.

Take the advantage of nano-technology. Nano-technology can create nano-structures with numerous grain boundaries. This can scatter phonons and then reduce phonon contribution of thermal conductivity. Consequently, ZT is enhanced through nano-technology [10-15]. For example, Poudel's group fabricated $Bi_xSb_{2-x}Te_3$ nano-powder in bulk with a high density of grain boundaries. Which can reduce phonon thermal conductivity to 0.4 W/m·K. As a result, ZT was enhanced to 1.4[16]. Xie's group used the μm/nm mixed structure concept to fabricate the $Bi_{0.5}Sb_{1.5}Te_3$ nano-composite through combining the single-element melt spinning and spark plasma sintering processes. The ZT can reach 1.5[17].

Moreover, few approaches for enhancing the Seebeck coefficient in Bi_2Te_3 have been reported. Sn doping in Bi_2Te_3 can increase the Density Of States (DOS), of the valence band near the Fermi energy due to the formation of a resonance state[18]. On the other hand, Faleev et al. presents a theory that can enhance Seebeck coefficient of semiconductor materials with metallic nanoinclusion[19]. Metal/semiconductor interfaces would create a band bending effect resulting in a low energy electrons filtering effect. They presented a theoretical model and numerical calculation of the Seebeck enhancement in a PbTe alloy with Pb nano-inclusions. This theoretical model has been proved through various thermoelectric nano-composites, including Bi_2Te_3/Te[20], PbTe[21] and PbTe/Pb[22]. Kim's group[20] fabricated Bi_2Te_3/Te by homogeneously dispersed to 15 nm Te nano-particles between $Bi_{0.5}Sb_{1.5}Te_3$ films. Which Seebeck coefficient increased from 169 to 248 μV/K. However, there was no observation of a carrier energy filtering effect made in the Bi_2Te_3 bulk.

Nano-composite and heat treatment methods were used in this report. Melt spinning and hot pressing processes were used to fabricate the $Bi_{0.5}Sb_{1.5}Te_3$ bulk in the nano-composite structure. The $Bi_{0.5}Sb_{1.5}Te_3$ nano-composite with the highest ZT was annealed to eliminate defects due to the hot pressing process. As a result, thermal conductivity reduction and Seebeck coefficient enhancements were observed on samples with and without the annealing process, respectively. Thereby enhance ZT.

2. EXPERIMENTAL METHOD

A $Bi_{0.5}Sb_{1.5}Te_3$ ingot was fabricated by using the zone melting method with stoichiometric Bi, Sb and Te. The $Bi_{0.5}Sb_{1.5}Te_3$ ingot was used as a baseline for all the studies. Part of the $Bi_{0.5}Sb_{1.5}Te_3$ ingot was ground into a powder with a particle size of between 45 and 75 μm stated as the Zone Melting Powder (ZMP). The other part of $Bi_{0.5}Sb_{1.5}Te_3$ was used to prepare the melt spun ribbon. The Melt Spun Powder (MSP) was ground to a particle size to within 10 μm. The $Bi_{0.5}Sb_{1.5}Te_3$ nano-composite powder was prepared by mixing various ratios of MSP (0, 20, 40, 100 wt%) and ZMP. The mixed $Bi_{0.5}Sb_{1.5}Te_3$ nano-composite powder was then hot pressed to form $Bi_{0.5}Sb_{1.5}Te_3$ nano-composite under a temperature of 400℃, in a vacuum of 100 Mpa (to $2*10^{-5}$ torr) for 30 minutes. All the nano-composite samples studied were summarized in Table 1. Sample E was obtained by annealing the sample C at 300℃ for 12 hours in a vacuum (to $2*10^{-5}$ torr).

Table 1 Summary of all the nano-composite samples

	A	B	C	D	E
x wt% melt spun powder	0	20	40	100	40
300℃ anneal, 12 hours	No	No	No	No	Yes

XRD data of all the studied samples was taken with the Bruker D8 X-ray powder diffraction instrument to within 5 to 100°. SEM imaging and EDS data were taken with the Zeiss Auriga FIB-SEM Instrument. The size of the nano-grains were measured with the FEI-Tecnai-G2-G20 Scanning Transmission Electron Microscope (STEM). Thermoelectric properties were measured with equipment developed by IOFFE. This equipment can directly measures electrical conductivity, Seebeck coefficient and thermal conductivity at the same time. Carrier concentrations and mobility of samples C and E were measured with the Ecopia HMS3000 Hall Measuring System.

3. RESULTS AND DISCUSSION

3.1 Melt spun ribbon

The optical and SEM image of typical melt spun ribbon is shown in Fig.1(a). Melt spun ribbon exhibits a silver color, where the typical length and width are 0.3 to 6 mm, 0.5 to 4 mm respectively. The surface contact with and without cooling roll are known as contact and free surfaces respectively. The SEM image of the

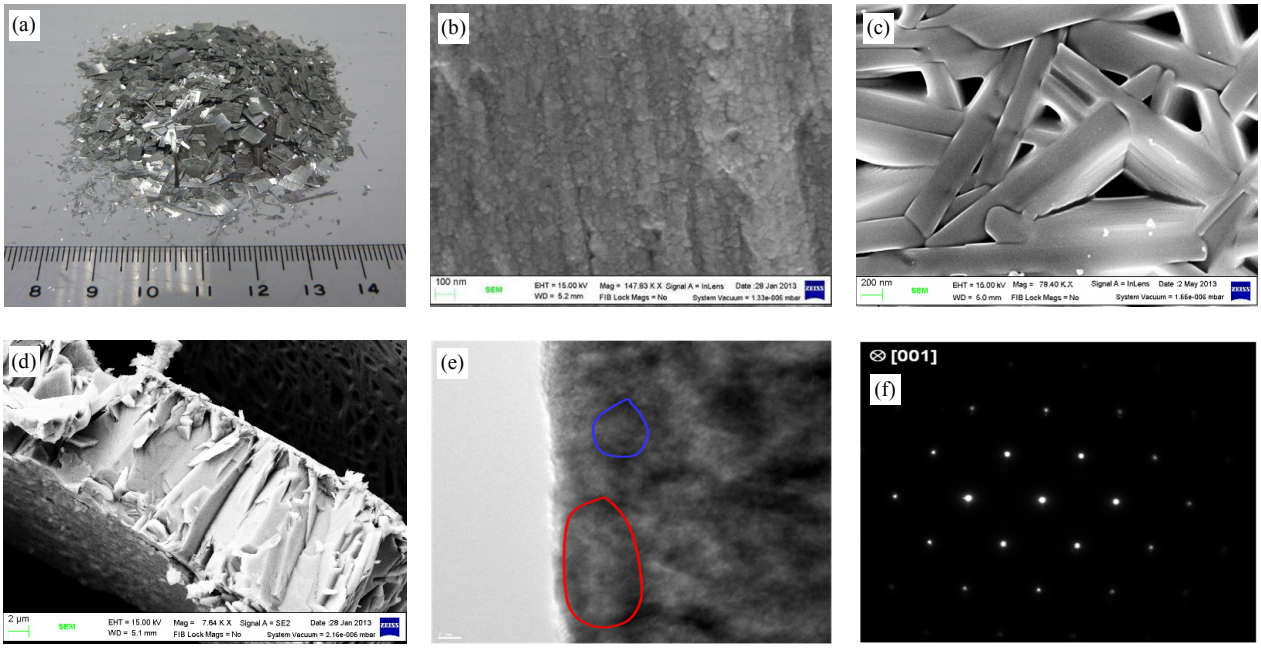

Fig.1. (a) Optical image of melt-spun ribbon. (b) SEM image of contact surface. (c) SEM image of free surface. (d) SEM image of side view. (e) TEM image of free surface of melt spun $Bi_{0.5}Sb_{1.5}Te_3$. (f) Back electron diffraction pattern of red circle in Fig.1(e).

contact surface shows that there are numerous nano-grains with a typical grain size of around 20 to 100 nm as shown in Fig.1(b). However, the SEM image of the free surface shows that there are stick-like structures as shown in Fig.1(c). Typical length and width of these stick-like structures are 0.2 to 3 μm and 100 to 300 nm respectively. From the triangular interspaces between the stick-like structures show that the stick-like structures are stacked by layers. Considering $Bi_{0.5}Sb_{1.5}Te_3$ belongs to a layered structure along the c-axis. This implies that the stick-like structures grow along ab-plane. The SEM side view of melt spun ribbon is shown in Fig.1(d). Typical thickness of melt spun ribbon is around 8 μm. The SEM side view shows that there are sticks perpendicular to the contact and free surface. Typical length and width of these sticks are 8 and 2 to 4 μm respectively.

A TEM was used to verify the details of the structure and grain size of Fig.1(b). The TEM image is shown in Fig.1(e). It suggests that the stick-like structure is composed of nano-grains with a grain size of around 5 to 10 nm. A similar grain size is also observed in the side view of the melt spun ribbon (not shown). Therefore, we suggest that the melt spun ribbon is composed of nano-grains. The back electron diffraction pattern of Fig.1(e) nano-grain is shown in Fig.1(f). The pattern shows a hexagonal arrangement, which means the structure of the $Bi_{0.5}Sb_{1.5}Te_3$ nano-grain is along the *c*-axis. That means the nano-crystalline $Bi_{0.5}Sb_{1.5}Te_3$ was fabricated successfully. However, TEM can only observe a local area not the whole region. Therefore, the average grain size is still based on the SEM image.

The XRD patterns of the $Bi_{0.5}Sb_{1.5}Te_3$ ingot, melt spun ribbon and hot pressed sample A to D are shown in Fig.2. No structural phase transition was observed after the melt spinning process and after the hot pressing process. However, after the melt spinning process, the preferred orientation was changed from (006) and (0015) of ingot to (110) and (205) of the MSP. Whereas, the preferred orientation was not observed after the hot pressing process.

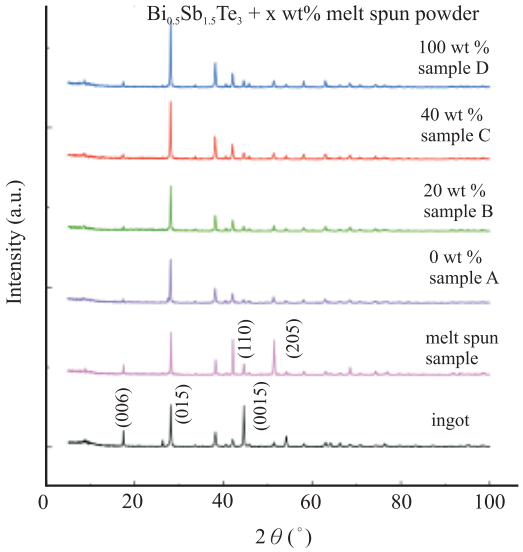

Fig.2. XRD data of $Bi_{0.5}Sb_{1.5}Te_3$ ingot, melt spun powder and samples A to D.

EDS data of the contact and free surface are summarized in Table 2. The Bi:Sb:Te ratio of the contact and free surface are similar. This means there is no segregation occurring on the melt spun ribbon. The Bi:Sb:Te ratio is close to 1:3:6, which is matched by the initial element ratio of the ingot. Combining it with the XRD data, it implies that the melt spinning process can quench the high temperature phase successfully without segregation.

3.2 Hot pressed sample (micro/nano-structure)

Typical SEM images of a fractured surface of hot pressed samples before the annealing process is shown in Fig.3. ZMP (~ 50 μm) is surrounded by smaller MSP (< 2 μm). There are numerous nano-grains (< 100 nm) in the enlarged fracture surface of the MSP as shown in Fig.3(b). The TEM image of the MSP shows that grain size is around 10 nm. Which is similar with the grain size of melt spun ribbon. Thus, the grain growth during the hot pressing process is limited.

Table 2 Weight and atomic percentages of contact surface and free surface of melt spun $Bi_{0.5}Sb_{1.5}Te_3$

Element	Contact		Free surface	
	Weight (%)	Atomic (%)	Weight (%)	Atomic (%)
Sb	26.83	29.19	27.37	29.77
Te	60.41	62.72	59.91	62.17
Bi	12.76	8.09	12.72	8.06
Total	100	100	100	100

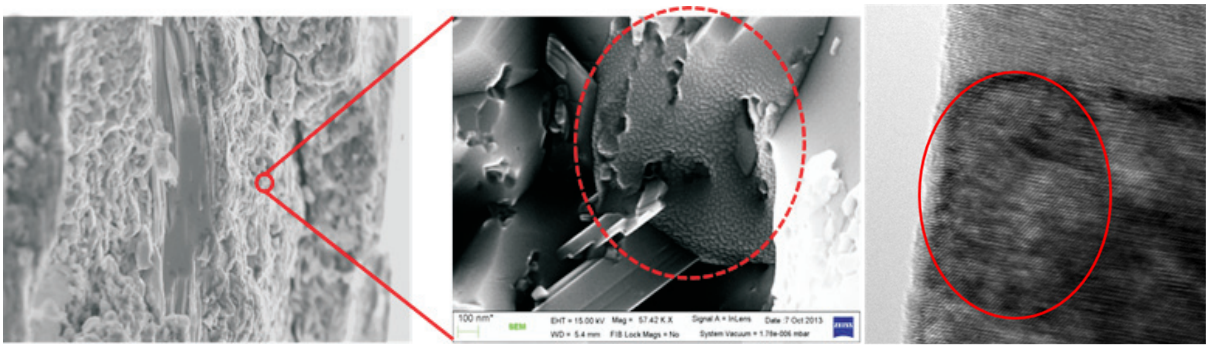

(a) (b) (c)

Fig.3. (a) SEM image of typical hot pressed $Bi_{0.5}Sb_{1.5}Te_3$ nano-composite. (b) Enlarged SEM image of Fig.3(a). Red circle shows nano grain of the MSP with grain size below 100 nm. (c) TEM image of hot pressed $Bi_{0.5}Sb_{1.5}Te_3$ nano-composite. Nano sized grain is shown in red circle. Which size is around 10 nm.

The Seebeck coefficient, electrical conductivity, thermal conductivity and ZT of $Bi_{0.5}Sb_{1.5}Te_3$ ingot and nano-composites are shown in Figs.4(a) to (d). The Seebeck coefficient peaks exist for all samples studied between 350 and 400 K. These peaks indicate the onset of bipolar conduction (minority carriers with opposite sign are excited into the conduction band). Comparing with the ingot, samples A, B and C show Seebeck coefficient enhancements. The reason could be the existence of the numerous grain boundaries.

Comparing with the electrical conductivity of the ingot and samples A to D at room temperature. The electrical conductivity decline of sample A and B to D are between 55 and 75%. Decline in electrical conductivity is mainly due to the existence of the numerous grain boundaries. That can scatter conducting

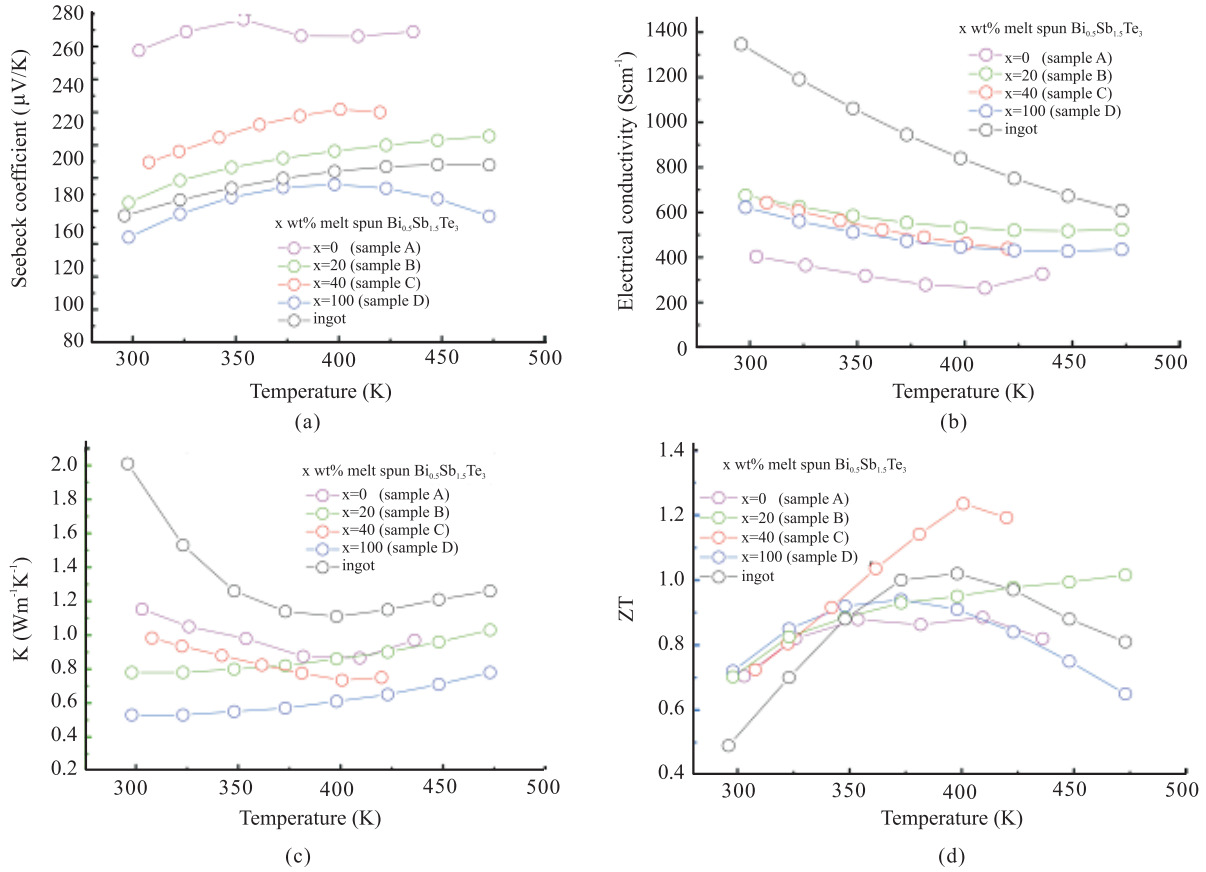

Fig.4. Temperature dependent (a) Seebeck coefficient, (b) Electrical conductivity, (c) Thermal conductivity and (d) ZT of $Bi_{0.5}Sb_{1.5}Te_3$ ingot and nano-composite with various melt spun ribbon (0, 20, 40, 100 wt%).

electrons while energy is lower than the energy gap of the grain boundaries. As the temperature increases, electrical conductivity of $Bi_{0.5}Sb_{1.5}Te_3$ nano-composite decreases slowly. The difference of electrical conductivity between ingot and nano-composite becomes smaller and smaller as temperature increases. The electrical conductivities are similar at temperatures above 400 K. This implies that the minority carriers dominant at temperatures above 400 K.

The thermal conductivity decreases as more melt spun ribbon is mixed within the $Bi_{0.5}Sb_{1.5}Te_3$ nano-composite. There is a 40 to 70% decline in thermal conductivity at room temperature. This is mainly due to high density grain boundaries and interfaces in the nano-composite. That results in phonon scattering and decreases thermal conductivity. Generally speaking, thermal conductivity becomes smaller with increasing temperature. However, while temperature above that of the Seebeck peak, the value of thermal conductivity becomes larger. The reason is also related with the existence of minority carriers.

The ZT of samples A to D are as shown in Fig.4(d). Although sample A and sample D have the highest Seebeck coefficient and thermal conductivity respectively, the poor electric conductivity or Seebeck coefficient results in poor ZT. Sample D has the highest value with ZT_{max} = 1.2 at 400 K, there is a 20% improvement compared with that of the ingot's ZT_{max}.

3.3 Micro/nano-structure and nano-precipitation

Sample C, with the highest ZT, was annealed to eliminate defects due to the hot pressing process. The SEM image of sample C shows the flat surface as shown in Fig.5(a). After the annealing process, sample E shows several dark regions at the surface as shown in the red circles of Fig.5(b). The distribution of these dark regions is not homogeneous. At high magnification, the dark regions are shown in Fig.5(c). Which are formed by the aggregated nano-particles with typical particle size of 15 to 20 nm (Fig.5(c)). EDS analysis of nano-particles shows Bi:Sb:Te ~ 2:6:92. This suggests the observed nano-particles were Te-rich nano-precipitations.

Electrical conductivity, Seebeck coefficient, thermal conductivity and ZT of sample C and sample E as a function of temperature are shown in Figs.6(a) and (b) respectively. For comparison with σ of sample C and E, σ decrease from 623 (sample C) to 610 (sample E) S/cm at T = 300 K. The carrier concentrations were 6.0 × 10^{19} and 8.2 × 10^{19} cm^{-3} for the samples C and E, respectively. The mobilities were to 165 and 156 cm^2/Vs for the samples without and with Te-rich nano-precipitations, respectively. The Seebeck coefficient of sample E increased by more than 20% from 190 to 236 μV/K at room temperature compared with sample C. The enhancement is shown in Figs.6(a) and (b) for the whole temperature range studied. The thermal conductivity of sample E decreased from 0.98 to 0.95 W/mK at room temperature. Therefore, ZT_{max} of sample C increases from 1.2 to 1.45 to that of sample E.

The presence of Te-rich nano-precipitations enhances the scattering of low energy electrons by the carrier energy filtering effect due to the barrier potential formed by the $Te/Bi_{0.5}Sb_{1.5}Te_3$ interfaces. Figure 7 shows the Seebeck coefficient as a function of the carrier concentration (Pisarenko plot) at room temperature. The solid line represents the calculated Seebeck coefficient as a function of the carrier concentration of nano-inclusion free $Bi_{0.5}Sb_{1.5}Te_3$ samples, based on a relaxation model at room temperature. There is a good similarity between the measured precipitation-free sample (blue solid circle) and the numerical calculated Seebeck coefficient of $Bi_{0.5}Sb_{1.5}Te_3$. The enhancement of the Seebeck coefficient of sample E with Te nano-precipitations was shown in the red circle. The dashed lines represent the numerically calculated room temperature Seebeck coefficient as a function of the carrier concentration of the sample. This is based on the theoretical simulation of the carrier energy filtering effect including 5 vol%

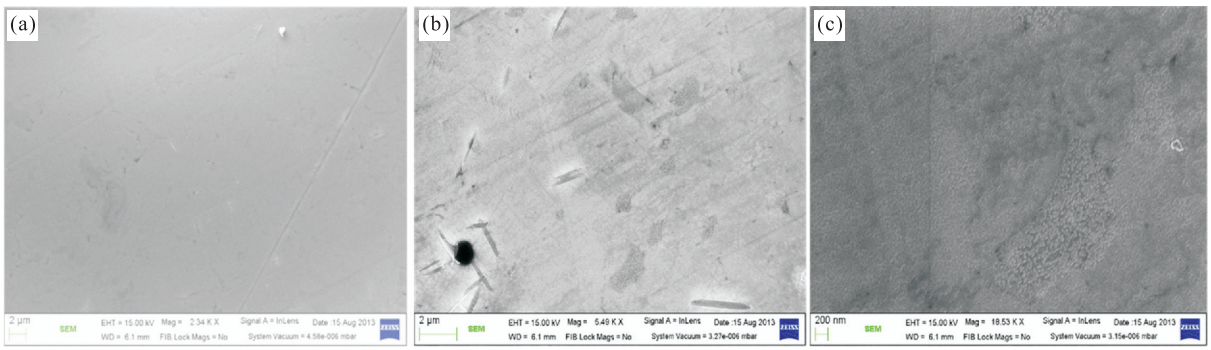

Fig.5. SEM images of (a) Sample C. (b) Sample E. (c) Partially enlarged region of sample E. Where red circles represent the observed aggregated Te nano-precipitations.

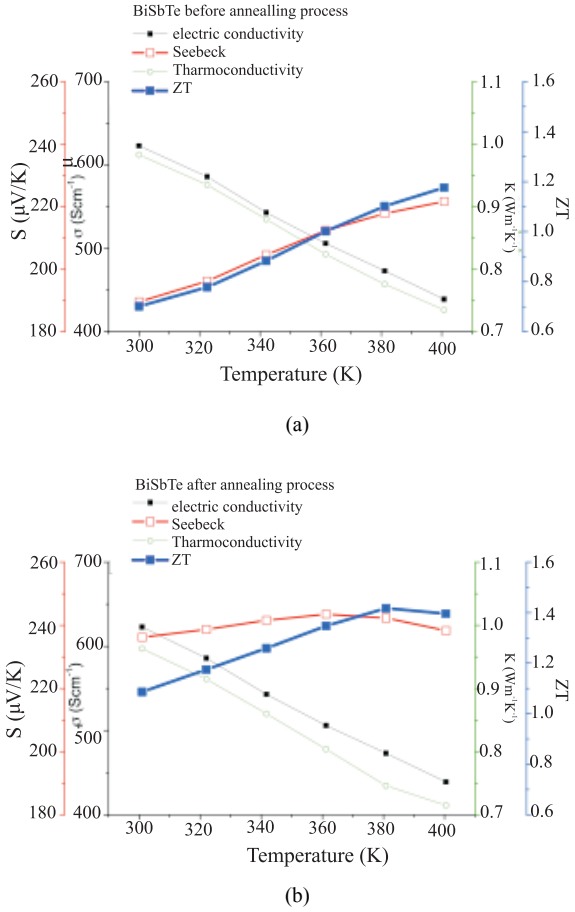

Fig.6. Electrical conductivity, Seebeck coefficient, thermal conductivity and ZT of (a) Sample C and (b) Sample E as a function of temperature.

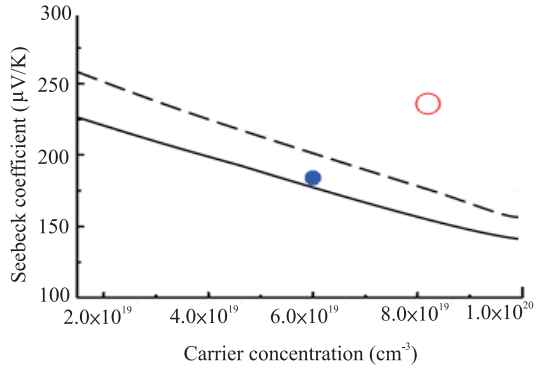

Fig.7. Seebeck coefficient as a function of the carrier concentration (Pisarenko plot) at room temperature for the Te nano-inclusion films, sample C (blue solid circle) and E (red circle). Solid line represents the calculation without nano-inclusion. The dashed line represents the numerical calculation with 5% nano-inclusion with a diameter of 15 nm.

nanoparticles with a diameter of 15 nm in a thin film, where the arrangement alternates nanoparticles and $Bi_{0.5}Sb_{1.5}Te_3$. The Seebeck coefficient of sample E is still higher than expectation of theoretical prediction. We speculate the deviation is a result of the size distribution and perfect dispersion.[20]

On the other hand, the carrier concentration and mobility usually reduce in the presence of Te-rich nano-precipitations. But the measured carrier concentrations increase with the presence of Te-rich nano-precipitations. We speculate the reason could result from the barrier potentials becoming overlapped in the case of aggregated Te-rich nano-precipitations due to the very short distances between nano-precipitations. Therefore that results in an enhanced carrier concentration. As a result, Seebeck coefficient shows a large enhancement for the sample with Te-rich nano-precipitations compared to that of the sample without Te-rich nano-precipitations.

4. CONCLUSIONS

(1) $Bi_{0.5}Sb_{1.5}Te_3$ nano-composites were fabricated by mixing various ratios (0, 20, 40 and 100 wt%) of micro-grain and nano-grain $Bi_{0.5}Sb_{1.5}Te_3$ powder. The highest ZT_{max} to 1.2@400K was obtained for a $Bi_{0.5}Sb_{1.5}Te_3$ nano-composite with a 40 wt% melt-spun nano-grain. There was a 20% improvement compared with that of the $Bi_{0.5}Sb_{1.5}Te_3$ ingot.

(2) The 20% improvement came from the significant reduction in thermal conductivity. The thermal conductivity reduction was a result of the phonon scattering due to the numerous grain boundaries formed by the nano-structure.

(3) $Bi_{0.5}Sb_{1.5}Te_3$ nano-composites were further annealed at 300℃ for 12 hours. The ZT was enhanced from 1.2 to 1.42. The micro-structure analysis showed there were aggregated Te-rich precipitations inside the $Bi_{0.5}Sb_{1.5}Te_3$ nano-composite, where grain sizes were ~15 to 20 nm.

(4) Te-rich precipitations result in the band bending effect and carrier energy filtering effect. These effects lead to a Seebeck coefficient enhancement and the improvement of the ZT.

(5) The microstructure of the $Bi_{0.5}Sb_{1.5}Te_3$ nano-composite shows that the melt spun powder exists at the grain boundary of the zone melting powder.

(6) The morphologies of contact and free surface of the melt spun ribbon show numerous nano-grain and stick-like shapes, respectively. Both are composed of 5 to 10 nm nano-grains.

REFERENCES

1. H. J. Goldsmid and R. W. Douglas: "The use of semiconductors in thermoelectric refrigeration", Br. J. Appl. Phys., 1954, vol. 5, p. 386.
2. D. L. Medlin and G. J. Snyder: "Interfaces in bulk thermoelectric materials. A review for Current Opinion in Colloid and Interface Science", Curr. Opin. Collid Interface. Sci., 2009, vol. 14, p. 226.
3. L. D. Chen, X. Y. Huang, M. Zhou, X. Shi and W. B. Zhang: "The high temperature thermoelectric performances of $Zr_{0.5}Hf_{0.5}Ni_{0.8}Pd_{0.2}Sn_{0.99}Sb_{0.01}$ alloy with nanophase inclusions", J. Appl. Phys., 2006, vol. 99, p. 064305.
4. J. Yang and R. Chen: "Thermoelectric properties of silver-doped n-type Bi_2Te_3-based material prepared by mechanical alloying and subsequent hot pressing", Journal of Alloys and Compounds, 2006, vol. 407, p. 330.
5. J. Yang, T. Aizawa, A. Yamamoto and T. Ohta: "Thermoelectric properties of p-type $(Bi_2Te_3)_x(Sb_2Te_3)_{1-x}$ prepared via bulk mechanical alloying and hot pressing", Journal of Alloys and Compounds, 2000, vol. 309, p. 225.
6. H. C. Kim, T. S. Oh and D. B. Hyun: "Thermoelectric properties of the p-type Bi_2Te_3-Sb_2Te_3-Sb_2Se_3 alloys fabricated by mechanical alloying and hot pressing", Journal of Physics and Chemistry of Solids, 2000, vol. 61, p. 743.
7. X. S. Zhou, Y. Deng, C. W. Nan and Y. H. Lin: "Transport properties of SnTe–Bi_2Te_3 alloys", Journal of Alloys and Compounds, 2003, vol. 352, p. 328.
8. E. Koukharenko, N. Frety, G. Nabias, V. G. Shepelevich and J. C. Tedenac: "Microstructural study of Bi_2Te_3 material obtained by ultrarapid quenching process route", Journal of Crystal growth, 2000, vol. 209, p. 773.
9. C. J. Liu, H. C. Lai, Y. L. Liu and L. R. Chen: "High thermoelectric figure-of-merit in p-type nanostructured $(Bi,Sb)_2Te_3$ fabricated via hydrothermal synthesis and evacuated-and-encapsulated sintering", J. Mater. Chem. 2012, vol. 22, p. 4825.
10. K. F. Hsu, S. Loo, F. Guo, W. Chen, J. S. Dyck, C. Uher, T. Hogan, E. K. Polychroniadis and M. G. Kanatzidis: "Cubic $AgPb_mSbTe_{2+m}$: Bulk Thermoelectric Materials with High Figure of Merit", Science, 2004, vol. 303, p. 818.
11. Y. Pei, A. D. LaLonde, N. A. Heinz, X. Shi, S. lwanaga, H. Wang, L. Chen and G. J. Snyder: "Stabilizing the Optimal Carrier Concentration for High Thermoelectric Efficiency", Adv. Materials, 2011, vol. 23, p. 5674.
12. M. Ohta, K. Biswas, S. H. Lo, J. He, D. Y. Chung, V. P. Dravid and M. G. Kanatzidis: "Enhancement of Thermoelectric Figure of Merit by the Insertion of MgTe Nanostructures in p-type PbTe Doped with Na_2Te", Adv. Materials, 2012, vol. 2, p. 1117.
13. J. H. Son, M. W. Oh, B. S. Kim, S. D. Park, B. K. Min, M. H. Kim and H. W. Lee: "Effect of ball milling time on the thermoelectric properties of p-type $(Bi,Sb)_2Te_3$", J. Alloy Compd., 2013, vol. 566, p. 168.
14. J. Jiang, L. Chen, S. Bai and Q. Yao: "Thermoelectric performance of p-type Bi–Sb–Te materials prepared by spark plasma sintering", J. Alloy Compd., 2005, vol. 390, p. 208.
15. X. A. Fan, J. Y. Yang, W. Zhu, S. Q. Bao, X. K. Duan, C. J. Xiao and K. Li: "Preferential orientation and thermoelectric properties of p-type $Bi_{0.4}Sb_{1.6}Te_3$ system alloys by mechanical alloying and equal channel angular extrusion", J. Alloy Compd., 2008, vol. 461, p. 9.
16. B. Poudel, Q. Hao, Y. Ma, Y. Lan, A. Minnich, B. Yu, X. Yan, D. Wang, A. Muto, D. Vashaee, X. Chen, J. Liu, M. S. Dresslhaus, G. Chen and Z. Ren: "High-Thermoelectric Performance of Nanostructured Bismuth Antimony Telluride Bulk Alloys", Science 2008, vol. 320, p. 634.
17. W. Xie, S. Wang, S. Zhu, J. He, X. Tang, Q. Zhang, and T. M. Tritt: "High performance Bi_2Te_3 nanocomposites prepared by single-element-melt-spinning spark-plasma sintering", J. Mater. Sci., 2013, vol. 48, p. 2745.
18. C. M. Jaworski, V. Kulbachinskii and J. P. Heremans: "Resonant level formed by tin in Bi_2Te_3 and the enhancement of room-temperature thermoelectric power", Phys. Rev. B 2009, vol. 80, p. 233201.
19. S. V. Faleev and F. Léonard: "Theory of enhancement of thermoelectric properties of materials with nanoinclusions", Phys. Rev. B, 2008, vol. 77, p. 214304.
20. S. II Kim, K. Ahn, D. H. Yeon, S. Hwang, H. S. Kim, S. M. Lee and K. H. Lee: "Enhancement of Seebeck Coefficient in $Bi_{0.5}Sb_{1.5}Te_3$ with High-Density Tellurium Nanoinclusions", Appl. Phys. Express, 2011, vol. 4, p. 091801.
21. K. Kishimoto, K. Yamamoto and T. Koyanagi: "Influences of Potential Barrier Scattering on the Thermoelectric Properties of Sintered n-Type PbTe with a Small Grain Size", Jpn. J. Appl. Phys., 2003, vol. 42, p. 501.
22. J. P. Heremans, C. M. Thrush and D. T. Morelli: "Thermopower enhancement in PbTe with Pb precipitates", J. Appl. Phys., vol. 98, p. 063703. □